

RESEARCH PAPER

Removal of Rhodamine B from Aqueous Solutions Using CS-g-p(AA-co-DEAP)/MWCNTs-COOH Hydrogel Nanocomposite as an Adsorbent

Makarim A. Mahdi, Layth S. Jasim *, Hayder O. Jamel

Department of Chemistry, College of Education, University of Al-Qadisiyah, Diwaniyah, Iraq

ARTICLE INFO

Article History:

Received 10 March 2025

Accepted 05 June 2025

Published 01 July 2025

Keywords:

Adsorption

Carboxylated multi-walled carbon nanotubes

Rhodamine B

Thermodynamic

ABSTRACT

This study investigates the performance of chitosan-grafted poly(acrylic acid-co-2-(((1E,2E)-1,2-diphenyl-2-((4(E-1-(thiazole 2yl imino) ethyl) phenyl) imino) ethylidene) amino) phenol/carboxylated multi-walled carbon nanotubes hydrogel nanocomposite (CS-g-p(AA-co-DEAP)/MWCNTs-COOH) for Rhodamine B (RhB) dye adsorption. The materials' adsorption process, thermal properties, and structural properties were studied using FT-IR, FESEM, TEM, TGA, and XRD analyses. Carbonyl and hydroxyl groups were found by FT-IR measurement. FESEM and TEM investigations showed a porous surface structure and surface shape changes after adsorption. Due to strong contacts between the copolymer, MWCNTs-COOH and efficient nanotube dispersion in the matrix, TGA studies showed that the hydrogel nanocomposite had enhanced heat stability. The composite hydrogel matrix had a well-dispersed and uniform distribution of MWCNTs-COOH. Equilibrium time was 120 min for adsorption. Dye adsorbed and equilibrium concentrations were represented by adsorption isotherms. The Langmuir, Freundlich, and Temkin isotherm models showed a high degree of consistency for RhB dye adsorption, indicating the heterogeneity of the adsorbent surface. The study finished by evaluating the temperature impacts on adsorption. Calculations showed that the adsorption process was exothermic and the contact between the adsorbent surface and dye molecules would diminish with temperature. The hydrogel nanocomposite's adsorption behavior, surface morphology, and heat stability were thoroughly investigated, suggesting their utility in dye removal applications.

How to cite this article

Mahdi M., Jasim L., Jamel H. Removal of Rhodamine B from Aqueous Solutions Using CS-g-p(AA-co-DEAP)/MWCNTs-COOH Hydrogel Nanocomposite as an Adsorbent. J Nanostruct, 2025; 15(3):928-942. DOI: 10.22052/JNS.2025.03.011

INTRODUCTION

Human activities in various industries, such as textiles, contribute to water pollution, through the discharge of dyes [1, 2]. These pollutants pose serious threats to both humans and other creatures. Rhodamine B (RhB), a highly toxic

dye prevalent in textile wastewater, is valued for its high stability and non-degradability in the textile industry as a textile dye [3-5]. RhB also finds usage in ballpoint pens, paints, leather, dye lasers, carbon paper, stamp inks, explosives, and fireworks[6-9]. Classified as a carcinogenic,

* Corresponding Author Email: layth.alhayder@gmail.com



neurotoxic dye, RhB induces respiratory and skin infections, gastrointestinal irritation, and eye infections[10-13]. It exhibits developmental toxicity and mutagenicity in animals and humans. Intensive use of RhB is toxic via inhalation and ingestion, causing liver and thyroid damage, and irritations to the eyes and skin. Hence, the dye's removal or reduction in water solutions is crucial[14]. Adsorption, a simple, easy, efficient, and relatively inexpensive method, is one of various ways to remove dyes [15-17]. In recent years, substantial research has been directed towards the use of nanoparticles as adsorbent materials [18-20]. Nanomaterials have responded well to the need for high-surface-area materials, high adsorption capacity, and low cost that can successfully remove pollutants even at low concentrations[21-23]. Specific materials, particularly hydrogel nanomaterials, are used to overcome traditional adsorbents' limitations[24]. The next generation of adsorbents (nano-adsorbents) for water treatment systems, with exceptional physical and chemical properties, make them superior adsorbent materials compared to their similar bulk counterparts[25]. MWCNTs-COOH have attracted significant interest in various fields, such as nanotechnology, materials science, and biomedical applications, due to their unique combination of the inherent properties of carbon nanotubes (strength, conductivity, etc.) and the reactivity of carboxyl groups[26-28]. The carboxyl groups can serve as attachment points for a variety of other molecules, enhancing the versatility and utility of these functionalized nanotubes. Moreover, MWCNTs-COOH can serve as effective adsorbents in environmental remediation due to their high surface area and the chemical reactivity of the carboxyl groups, which can interact with various contaminants[29]. These properties, among others, make MWCNTs-COOH a promising material for a multitude of applications[30]. This article aims to offer an extensive overview of the adsorption process of RhB onto CS-g-p(AA-co-DEAP)/MWCNTs-COOH hydrogel nanocomposite surface, discussing its synthesis, characterization, and potential application in dye removal.

MATERIALS AND METHODS

Chemicals

High-purity chemicals used in this study, such as Acrylic acid (AA), Chitosan (CS), acetic acid, hydrochloric acid, sodium hydroxide, N,N-

methylene-bis-acrylamide (MBA), potassium persulfate (KPS), 2-(((1E,2E)-1,2-diphenyl-2-((4(E-1-(thiazol-2-ylimino) ethyl) phenyl) imino) ethylidene) amino) phenol (DEAP), Carboxylated multi-walled carbon nanotubes (MWCNTs-COOH) and Rhodamine B (RhB) were supplied by Sigma Aldrich.

Synthesis of CS-g-p(AA-co-DEAP)/MWCNTs-COOH hydrogel nanocomposite

The polymerization in an aqueous solution was conducted by dissolving 0.5g of CS in 20 mL 1% acetic acid for 30 min with stirring and nitrogen gas for 15 min. The temperature of this solution was then raised to 60°C. After that, KPS (0.05g dissolved in 2mL distilled water) was added during 10 min, in which stirring was continued and nitrogen gas was administered for an additional 10 min. Post this procedure, the solution was cooled to 25°C. Sequentially, 5g of AA was introduced to the solution with continuous stirring. This was followed by the addition of 0.1g of DEAP (dissolved in 2mL ethanol) for 15 min and 10 mL of MWCNTs-COOH (0.1%), with constant stirring. Subsequently, 0.05g of MBA (dissolved in 2ml distilled water) was added to the solution over 10 min, while stirring and administering nitrogen gas for an additional 20 min. This prepared solution was transferred into plastic bottles and placed in a water bath at 60°C for three hours. The resulting compound was cut into small pieces, washed with distilled water to remove any reactive substance, and then oven-dried at 70°C until a constant weight was achieved for further experiments. This process is illustrated in Fig. 1.

Characterisation

The prepared samples were characterized using several instruments including field emission scanning electron microscopy (FESEM), transmission electron microscopy (TEM), thermogravimetric analysis (TGA) and X-ray diffraction (XRD), which were conducted in the Central Analytical Laboratory of KAC. Fourier transform infrared spectroscopy (FTIR) analyses were carried out at the University of Al-Qadisiyah laboratories.

Preparation of standard solutions of RhB dye

The standard solution of RhB dye used in this study was prepared at a concentration of 200 mg L⁻¹ by dissolving 0.2 g of the dye in 1 L of deionized

water. From this, various solutions with different concentrations were prepared.

Determination of maximum wavelength and calibration curve for RhB dye

The UV spectrum of RhB dye solutions in water at concentrations of 10 mg L⁻¹, was recorded. Absorption spectra were obtained using a UV-Vis spectrophotometer within the range of 200-800 nm. The λ_{max} for RhB dye was found to be 554 nm. The calibration curve for RhB dye was determined by preparing a series of solutions with consecutive dilutions of the standard RhB dye solution at concentrations ranging 1-10 mg L⁻¹, using a UV-Visible spectrophotometer. The absorbance of these solutions was recorded at the maximum absorption wavelength of 554 nm for the dye[31]. A calibration curve was obtained by plotting the absorbance values against the concentrations. Effect of adsorbent weight on a series of weights ranging from 0.001 to 0.1 g of surface with 10 mL of dye solution (200 mg L⁻¹) was studied [32]. The mixture was then placed in a shaker for 120 min at 25°C to reach equilibrium. Absorbance was measured after centrifugation at 6000 rpm for 15 min. The results were plotted as the amount adsorbed against the weight of the adsorbent to determine its effect on the adsorption process.

Equilibrium time for adsorption process

The equilibrium time for dye adsorption on the adsorbent surface was determined by fixing all conditions, including temperature (25°C), pH, dye concentration, and surface weight [33]. A solution of 200 mg L⁻¹ RhB dye was prepared and 10 mL of the dye solution was mixed with 0.05 g of the composite. The mixture was placed in a shaker at 25°C under various durations (1-240 min). The absorbance of the solutions was measured after separation to determine the optimal time for the adsorption process.

Adsorption isotherms

Different concentrations of the dye (5-200 mg L⁻¹) were prepared and 10 mL of each was added to 0.05 g of the adsorbent. The mixtures were placed in a shaker at a speed of 120 rotations per min (120 min) at a temperature of 25°C. The samples were then centrifuged, and their absorbance was measured using a UV-Visible spectrophotometer. The quantity of RhB dye uptake at equilibrium q_e (mg g⁻¹) was determined using the following Eq. 1 [34]:

$$q_e(\frac{mg}{g}) = \frac{V(C_o - C_e)}{m} \tag{1}$$

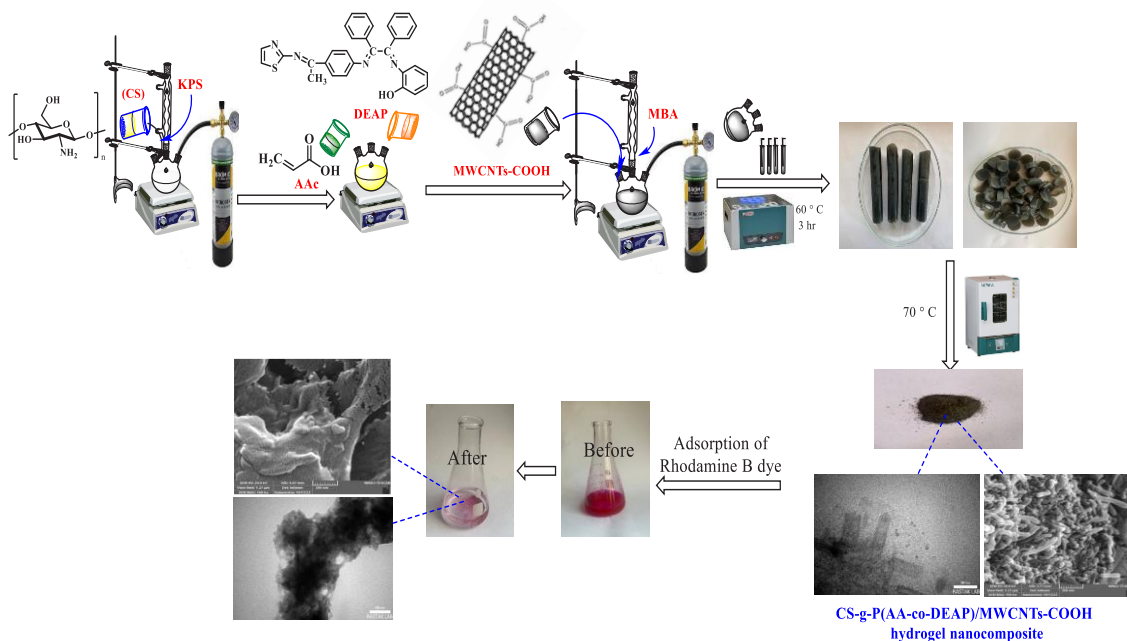


Fig. 1. Schematic illustrating the steps for preparing CS-g-p(AA-co-DEAP)/MWCNTs-COOH hydrogel nanocomposite.

Where C_o (mg L^{-1}) refers to the initial concentration of the dye. C_e (mg L^{-1}) represents the dye concentration at equilibrium. V (L) stands for the solution volume. m (g) is the weight of CS-g-p(AA-co-DEAP)/MWCNTs-COOH hydrogel nanocomposite. By employing equation (1), researchers can evaluate the effectiveness of dye adsorption using CS-g-p(AA-co-DEAP)/MWCNTs-COOH under various experimental conditions.

Effect of temperature

To determine the effect of temperature on the amount of substance adsorbed from aqueous solutions, the study was conducted on the RhB dye at diverse temperatures such as 15, 20, 25, and 30°C. 0.05 g of the composite was introduced into different concentrations (50-500 mg L^{-1}) of RhB in 10 mL of the dye solutions. The mixtures were placed in a shaker for 120 min, separated using a centrifuge and the absorbance was measured using a UV-Visible spectrophotometer.

Effect of acidity function

The effect of acidity function on the adsorption process was studied by employing 0.05 g of the sample and a concentration of 200 mg L^{-1} of RhB dye at different acidity function values (2-10) at a temperature of 25°C and duration of 120 min. The acidity function was adjusted using 0.1 M of

hydrochloric acid solution and 0.1 M of sodium hydroxide solution. The pH values were measured using a pH meter. The results were analyzed by plotting the amount of adsorbed substance against the acidity function values.

RESULTS AND DISCUSSION

FT-IR

The hydrogel nanocomposites prepared before and after adsorption of RhB dye were analyzed using FT-IR spectra within a range between (400-4000 cm^{-1})[35]. It also showed the synergy between the atoms around the sites of the packages shown by the active functional groups, such as the carbonyl and hydroxyl groups in the acidic carboxyl group, the amine and carbonyl groups in the amide group, and other effective functional groups[36-38]. The characteristic bands of MWCNTs-COOH were observed in the composite's FT-IR spectrum of Fig. 2a. The bands at 1719 cm^{-1} and 1197 cm^{-1} , corresponding to the stretching vibrations of C=O and C-O-C, respectively, indicating the presence of carboxyl groups on the surface of CNT. FT-IR spectrum in Fig. 2b displayed characteristic bands associated with the Schiff base (DEAP). The absorption bands at 1643 cm^{-1} and 1529 cm^{-1} were attributed to the stretching vibrations of the C=N and C=C groups, respectively[39-43]. The presence of a broad absorption band around

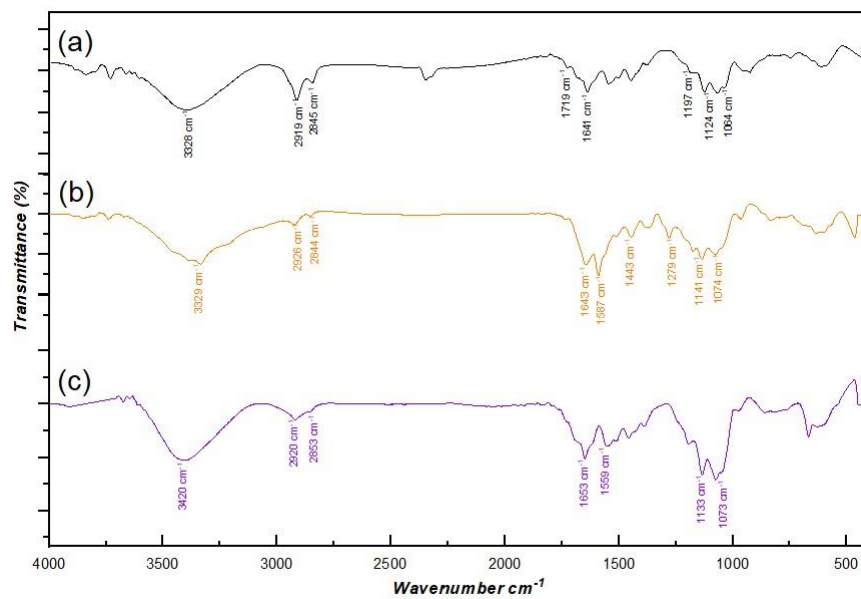


Fig. 2. FTIR spectra of the MWCNTs-COOH(a), DEAP(b)and CS(c).



3329 cm^{-1} was indicative of the -OH group in the phenol moiety. FTIR spectrum of chitosan in Fig. 2c showed the appearance of the hydroxyl group at 3440 cm^{-1} with an overlap with the NH group, as for the bending frequencies of the methylene and methyl, they appeared at 1380 cm^{-1} and 1427 cm^{-1} , respectively.

The FT-IR spectrum of the CS-g-p(AA-co-DEAP)/MWCNTs-COOH composite in Fig. 3a revealed the formation of the composite, as compared to the individual components. A shift in the -OH and -NH₂ stretching vibrations to lower wavenumbers, along with a decrease in the intensity of the carbonyl stretching band, suggested the involvement of these functional groups in complex formation. Additionally, the appearance of a new band at 1557 cm^{-1} indicated the presence of the coordinated Schiff base DEAP [44]. The FTIR spectra of the CS-g-p(AA-co-DEAP)/MWCNTs-COOH hydrogel nanocomposite before and after RhB adsorption revealed significant changes in the characteristic absorption bands, indicating interactions between the adsorbent and RhB. The shifts in the -OH, -NH₂, and carbonyl stretching vibrations suggested the involvement of these functional groups in the adsorption process. Based on the FTIR analysis, the adsorption of RhB onto the composite occurred via hydrogen bonding, electrostatic interactions, and π - π stacking between the dye molecules and the adsorbent's functional groups. The presence of MWCNTs-COOH in the composite contributed to the enhanced adsorption capacity

due to their large surface area and strong affinity for RhB molecules[45]. The observed changes in the absorption bands in Fig. 3b supported the proposed adsorption mechanism, highlighting the potential of the synthesized composite in RhB removal from aqueous solutions.

FESEM and TEM analyses

The FE-SEM technique was employed to investigate the surface characteristics of synthesized materials, enabling the assessment of particle shape, size, aggregation, and surface nature (porous or smooth) [46, 47]. Furthermore, it facilitated the examination of component homogeneity, distribution on the surface, and interconnection of polymer chains[48]. The incorporation of MWCNTs-COOH into the CS-g-p(AA-co-DEAP) appeared to enhance the porous structure, which may contribute to the composite's increased adsorption capacity for RhB. The FE-SEM images in Fig. 4(a and b) indicate an increase in surface smoothness resulting from the complete filling of surface pores by dye molecules. Consequently, the surface becomes entirely covered by the dye molecules, confirming the adsorption process[49]. The TEM images reveal valuable insights into the surface composition and response to the adsorption process[50]. The TEM analysis depicted in Fig. 4(c and d) demonstrates that CS-g-p(AA-co-DEAP)/MWCNTs-COOH hydrogel nanocomposite is dispersed particles that are uniformly distributed

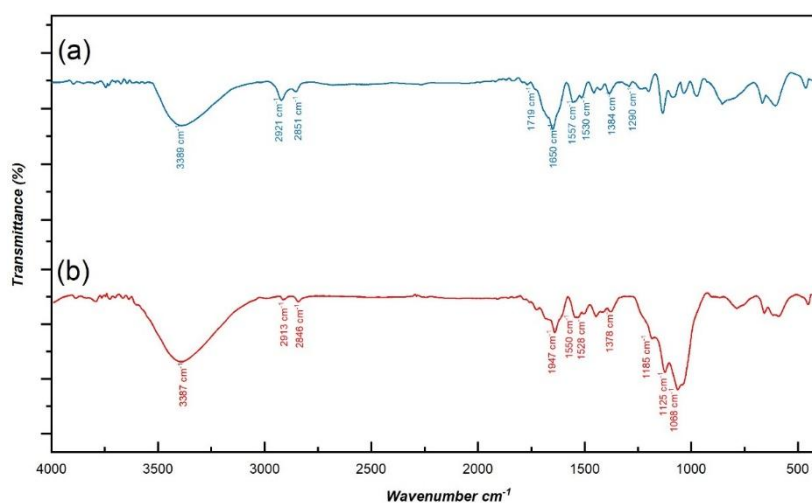


Fig. 3. FTIR spectra of the CS-g-p(AA-co-DEAP)/MWCNTs-COOH before and after (RhB) dye adsorption (a, b).

and regularly arranged[51]. Additionally, the presence of some agglomerates is noted. The surfaces are characterized by the formation of thin layers, which contribute to their overall structure. Upon the occurrence of the adsorption process, several changes in surface morphology are observed. Firstly, an increased presence of agglomerates with larger sizes is detected[52]. This phenomenon is attributed to the interference between dye molecules and surface molecules during the adsorption process[53]. Secondly, the thin layers of overlying materials diminish, due to the absorption and accumulation of dye molecules that penetrate the pores and grooves on the surface[54].

TGA Analysis

TGA curves of the sample heated in the presence of nitrogen gas within the temperature range of 40-800°C at a rate of 10°C min⁻¹ are showed in Fig. 5 [55, 56]. The TGA curve of MWCNTs-COOH was thermally stable, and the mass loss was only 6.4% in the temperature range of 60–700 °C, which can be regarded as the content of carboxyl functional groups[57].The

thermal characteristics of CS-g-p(AA-co-DEAP) and CS-g-p(AA-co-DEAP)/MWCNTs-COOH hydrogel nanocomposite demonstrated similar degradation profiles with curves disintegrated in three steps. The first degradation of 7.1% occurred in the temperature range of 60–200 °C due to the loss of water residual. In the temperature region of 200–300°C, there was a second decomposition stage of about 28.4% due to degradation of CS. In the third degradation profile, about 40.3% weight reduction occurred in the temperature range of 300–500°C due to the breaking of its carboxyl from acrylic acid groups and the cleavage of Schiff base linkages and degradation of the residual polymer[58]. The TGA curves revealed that the thermal stability and decomposition behaviour of hydrogels are strongly influenced by factors such as the nature of the monomers, crosslinking density, and the presence of functional groups[59]. The TGA results showed a significant improvement in the thermal stability of the CS-g-p(AA-co-DEAP)/MWCNTs-COOH hybrid materials compared to the pristine CS-g-p(AA-co-DEAP)[60]. The decomposition process occurred in multiple stages, corresponding to the degradation of the chitosan backbone, the loss

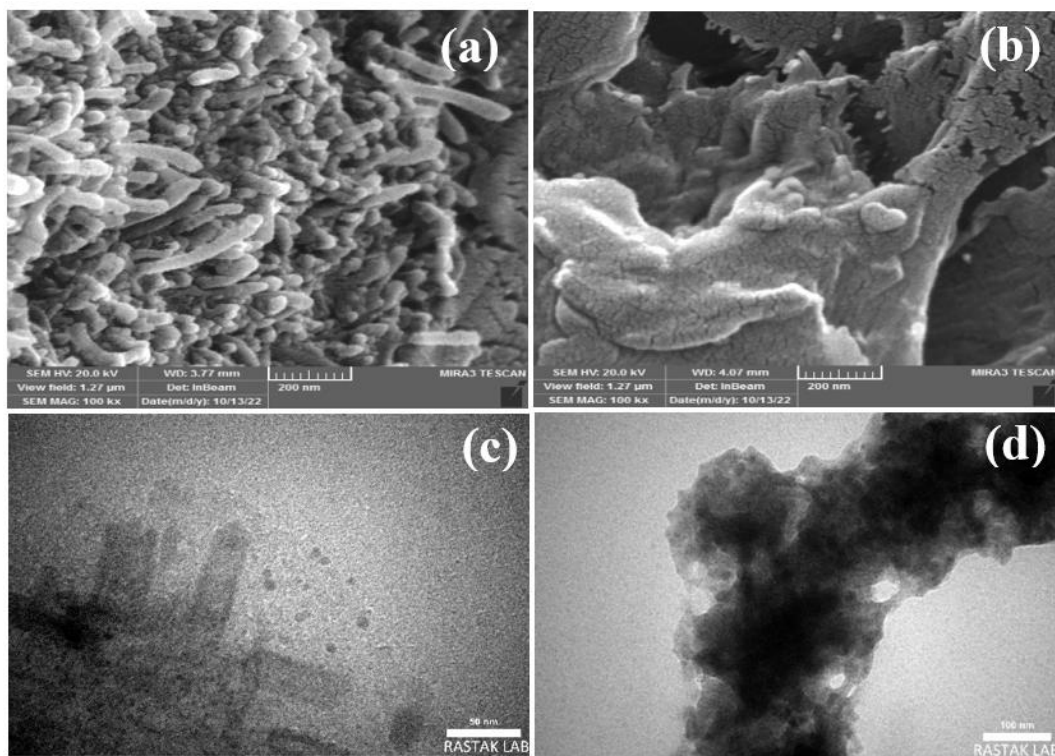


Fig. 4. FESEM and TEM images of nanocomposites: (a and c) before adsorption, and (b and d) after adsorption of RhB dye

of grafted poly(acrylic acid) chains, DEAP and the decomposition of MWCNTs-COOH. The enhanced thermal stability could be attributed to the

strong interactions between the copolymer and MWCNTs-COOH, as well as the efficient dispersion of the nanotubes within the matrix[61].

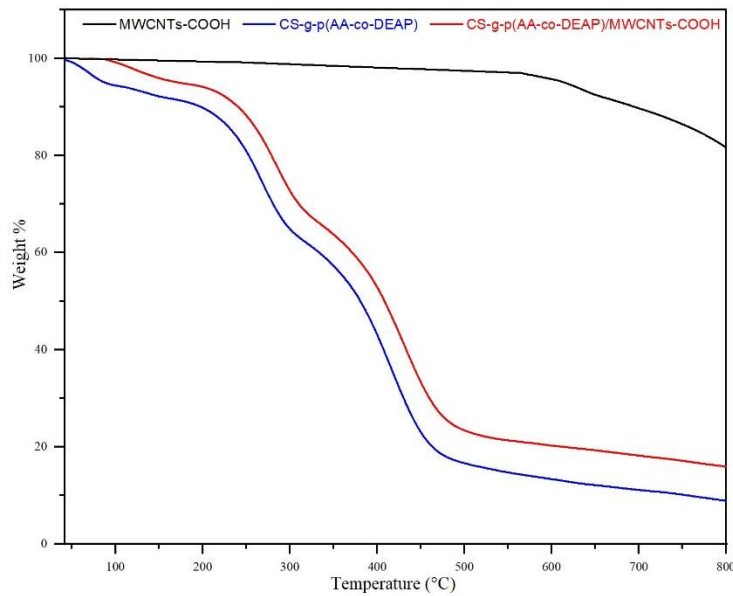


Fig. 5. TGA curves of the MWCNTs-COOH, CS-g-(PAA-co-DEAP) and CS-g-p(AA-co-DEAP)/MWCNTs-COOH.

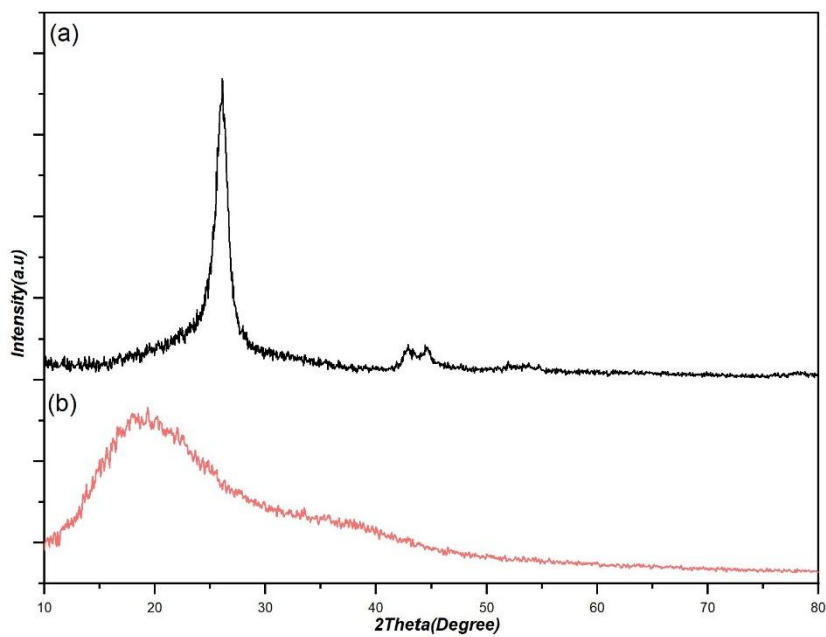


Fig. 6. XRD patterns of (a) MWCNTs-COOH and (b) CS-g-p(AA-co-DEAP)/MWCNTs-COOH.

XRD results

XRD measurement were used to study the crystal structure of MWCNTs-COOH and CS-g-p(AA-co-DEAP)/MWCNTs-COOH hydrogel nanocomposite [62, 63]. Generally, it is clear from the Fig. 6a that the MWCNTs-COOH exhibit three peaks; one at 26.1° ($d = 3.41 \text{ \AA}$), is attributed to the distance between walls in MWCNTs-COOH and others at 42.7° ($d = 2.10 \text{ \AA}$), and at 44.5° ($d = 2.02 \text{ \AA}$) are corresponded to the MWCNT interwall spacing, which can be indexed as the (002) plane of the graphitic carbon (JCPDS-ICDD No. 751621), (100) and (101) reflections of the carbon atoms, respectively[64]. Fig. 6b displays the XRD pattern of the CS-g-P(AA-co-DEAP)/MWCNTs-COOH composite hydrogels. The MWCNTs-COOH diffraction values suggest a well-dispersed and uniform distribution of MWCNTs-COOH in the composite hydrogel matrix. This dispersion alters the crystalline nature to a non-crystalline state, as evidenced by the decreased diffraction peak and the increased interlayer distance. The increase in interlayer distance is attributed to the penetration of organic molecules into the interlayer spaces, confirming the capacity of the nanostructures to accommodate structural deformations and swelling[65, 66].

Adsorption process

Effect of catalyst weight

Various weights were taken from the prepared

CS-g-PAA\DEAP composite ranging from)0.1 g to 0.005 g), at a constant concentration of 200 ppm for the RhB dye. 10 mL of the dye solution was added to the prepared weights at a temperature of 25°C . The results in Fig. 7 indicated that the removal percentage (Re%) of RhB dye increases with an enhancement in the weight of the adsorbent material, due to an increase in the surface area and consequently an increase in the number of active sites for the adsorbent material.

The impact of the MWCNTs-COOH concentrations (ranging from 0.01 to 0.3 wt%) used in the synthesis of the CS-g-PAA/DEAP/MWCNTs-COOH composite on the adsorption process was examined. At a constant weight of the composite (0.05g) at 25°C , 10mL of RhB dye solution with a fixed concentration of 200ppm was added. The results, as depicted in Fig. 8, indicate that the optimal concentration of MWCNTs-COOH is 0.1%. An increase in the proportion of MWCNTs-COOH in the composite leads to an increase in hydrophilic aggregates. Furthermore, the uniform dispersion of MWCNTs-COOH within the hydrogel would affect the structural composition of the hydrogel network due to its nanoscale structural nature. Consequently, a gradual increase in the quantity of adsorption occurs as the concentration of MWCNTs-COOH increases until it reaches a point where the amount of adsorption decreases. This decline can be attributed to the fact that excessive augmentation in MWCNTs-COOH substrates

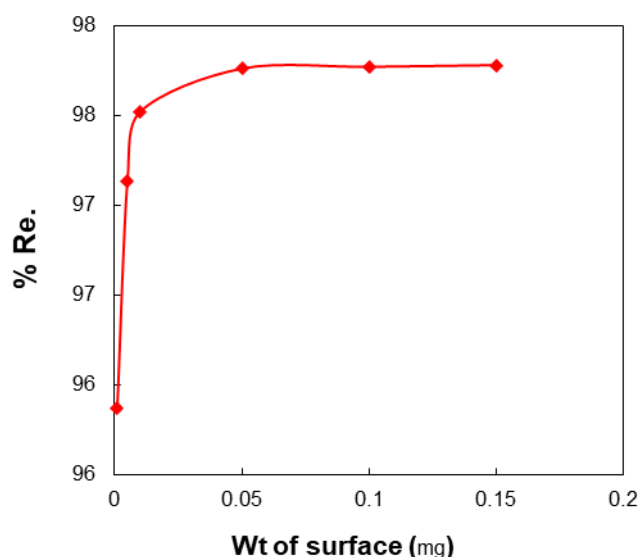


Fig. 7. Effect of composite weights on the adsorption of RhB dye at 25°C .

leads to the formation of agglomerates. These agglomerates tend to weaken the interaction between MWCNTs-COOH and the hydrogel network.

Equilibrium time

The appropriate equilibrium time for the

removal of a specific concentration of RhB dye by the adsorbent surface was studied at 25°C, pH=7, a constant adsorbent weight of 0.05g, and dye concentration of 200ppm for different time intervals ranging from 1 to 240 min. According to the results depicted in Fig. 9, the necessary equilibrium time for RhB dye is 120 min. During

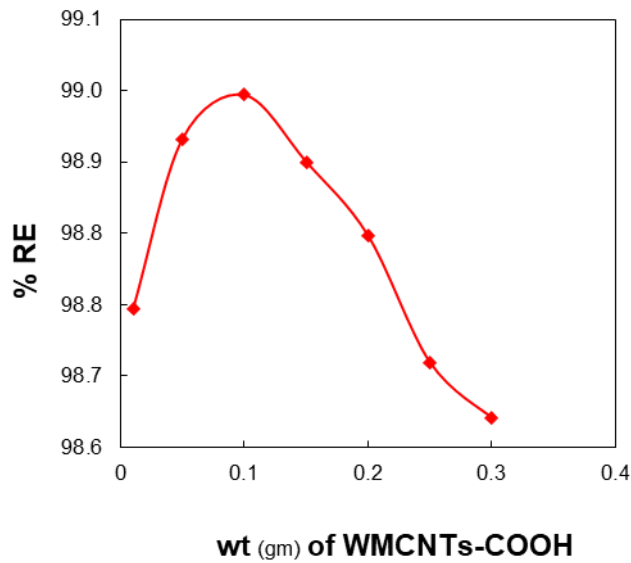


Fig. 8. Effect of MWCNTs-COOH weight on the adsorption of RhB dye at 25°C.

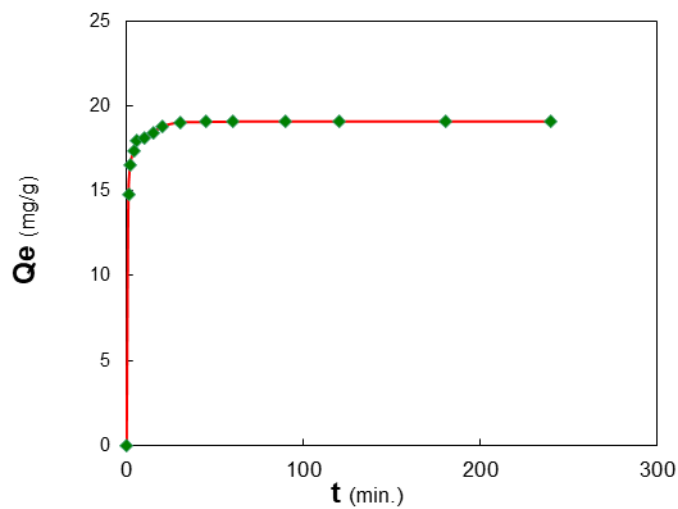


Fig. 9. Effect of time change on the amount of adsorbent for RhB dye at 25°C and pH=7.

the adsorption process, the quantity of adsorbed dye rapidly increases, followed by a gradual increment until the equilibrium time is reached. This quick increase in the adsorbed dye quantity is due to the large number of unoccupied active centers at the beginning of the adsorption process, which is sufficient for dye adsorption. Following this, the adsorption process becomes slower and more challenging due to all the active centers of the adsorbent surface being occupied by dye molecules.

Adsorption isotherms

Adsorption isotherms were studied to describe the relationship between the amounts of dye adsorbed (Q_e) on the composite surface and its equilibrium concentration (C_e). Based on the information obtained from the study and according to Giles classification, the results indicated that the adsorption process for the RhB dye corresponds to the L_4 type, also known as Langmuir type 4, where adsorption occurs in a monolayer, and the orientation of the adsorbed molecules is horizontal on the adsorbent surface[67]. Langmuir, Freundlich, and Temkin isotherm models were applied to describe the adsorption properties of the adsorbent materials used for the removal of

pollutants from the environment. As shown in Table 1 and Fig. 10, Freundlich’s isotherm shows a high degree of correspondence for the adsorption of RhB dye, as evidenced by the correlation coefficient (R^2) value of 0.9884, which indicates the heterogeneous nature of the adsorbent surface. According to Freundlich’s equation, the adsorption is not confined to a single molecular layer, but it is multilayered.

Effect of temperature and calculation of thermodynamic functions of the adsorption process

The adsorption process of RhB dye was performed on the surface of the composite at varying temperatures (15, 20, 25, and 30°C), and at concentrations within the range of 25-200 mg L⁻¹. It has been noted that temperature plays a significant and principal role in the adsorptive ability of the composite surface to adsorb dye from its aqueous solutions[68]. The obtained results suggest a decline in the amount of adsorbed dye (RhB) as temperatures escalate, as depicted in Fig. 11 and Fig. 12. It is deduced that the adsorption process is exothermic. This can be attributed to the rise in temperature, which enhances the solubility of adsorbed dye particles in the solvent,

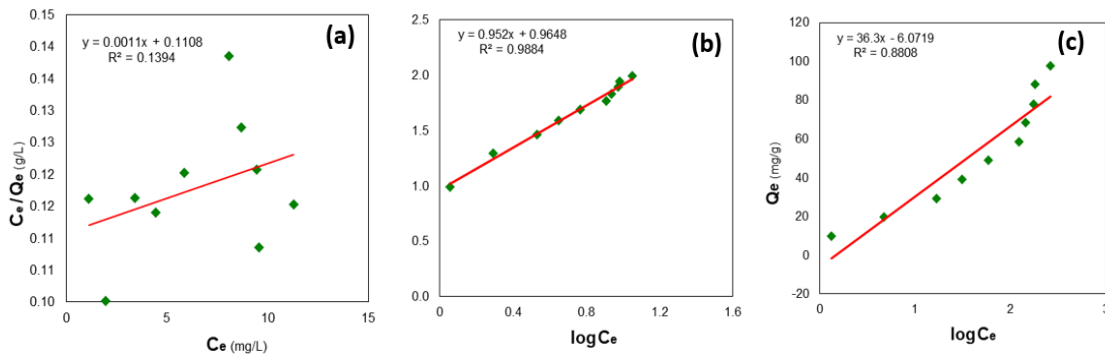


Fig. 10. Langmuir(a), Freundlich(b), and Temkin(c) isotherms for adsorption of RhB dye on the adsorbent surface.

Table 1. Correlation coefficients and constants for Langmuir, Freundlich, and Temkin isotherms for RhB dye adsorption on the surfaces of the composites.

| LANGMUIR | | | FREUNDLICH | | | TIMKEN | | |
|----------|----------|--------|------------|--------|--------|--------|------|--------|
| K_L | q_m | R^2 | K_F | n | R^2 | K_T | b | R^2 |
| 0.0099 | 909.0909 | 0.1394 | 9.2214 | 1.0504 | 0.9884 | 0.8459 | 36.3 | 0.8808 |



consequently diminishing the dye particles' adsorption affinity towards the adsorbent surface. Furthermore, increasing temperatures boost the kinetic energy of adsorbed molecules towards the adsorbent surface, leading to an augmentation in the system's entropy (ΔS). This corresponds to a decline in the system's order, which refers to the movement of adsorbed substance molecules on the adsorbent surface. This results in a weaker attraction between dye molecules and active sites on the adsorbent surface[69].

Thermodynamic functions were calculated by studying the impact of temperature on the adsorption process (ΔG free energy, ΔH enthalpy, ΔS entropy), due to their significance in understanding the adsorption process[70, 71]. These functions provide a detailed description of the dye molecule arrangement resultant from molecular interactions, as observed by measuring ΔS entropy changes. Additionally, by measuring ΔH enthalpy changes, it becomes possible to identify the dominant forces, whether chemical or physical

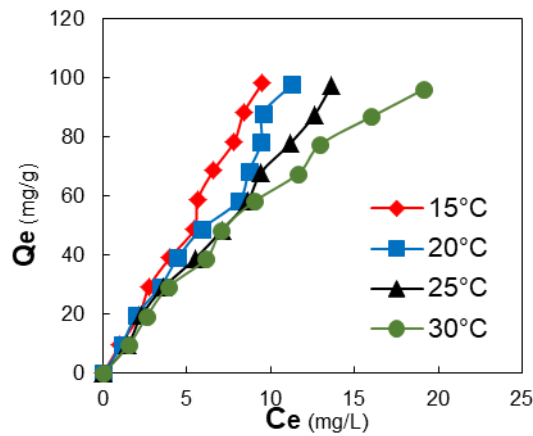


Fig. 11. Effect of temperature on RhB dye adsorption by composite surface at different temperatures (t=120 min, V=10 mL, wt=0.05).

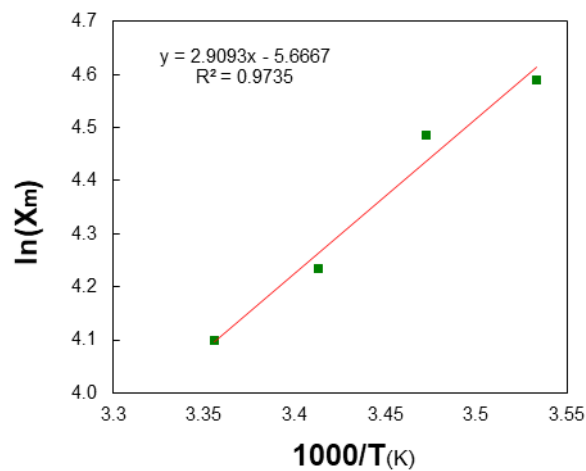


Fig. 12. Plot of $\ln(X_m)$ vs. inverse absolute temperature for RhB dye adsorption on composite surface.

and the reaction's direction. Table 2 illustrates thermodynamic function values for the dye adsorption process. The negative value of the heat content ΔH indicates that the RhB dye adsorption process is an exothermic process. This signifies that the mutual action between the adsorbent surface and dye molecules is expected to decrease with increase in temperature factor, which can be attributed to the disruption of bonds formed between the active centers of the adsorbent surface and dye molecules[72]. The negative value of the free Gibbs energy also indicates that the RhB dye adsorption process is spontaneous under the conditions in which the adsorption was conducted. Moreover, the negative value for the entropy change in the RhB dye adsorption suggests a reduction in the degrees of freedom for the adsorbed molecules, implying that these molecules are more constrained and ordered. The RhB dye adsorption is considered physical adsorption because the ΔH value is less than 40 KJ/mol[73].

Effect of pH function on adsorption

The influence of acidity function on the

adsorption process of RhB dye on the prepared adsorbent composite surface at a concentration of 200 mg L⁻¹ was studied. Acidity function values ranged from 2 to 10 while temperature and equilibration time conditions were fixed. The results, as shown in Fig. 13, indicate that the amount of dye adsorbed on the composite surface increases with the rise of acidity function[74]. This is attributed to the ionization of -COOH, and OH groups at high pH, making the composite surface negatively charged. This induces an electrostatic attraction between the positively charged dye molecules and the composite surface, enhancing the adsorption process. Also, repulsion between negative groups on the composite surface increases swelling, allowing dye molecules to diffuse into the composite surface, thereby enhancing adsorption[75]. Conversely, at low pH, high concentrations of H⁺ ions in the solution lead to competition between them and the positively charged dye molecules for active sites, decreasing adsorption[76]. Furthermore, at low pH, the composite surface groups -COOH, OH are protonated, leading to hydrogen bonding between polymer chains and carbon nanotubes,

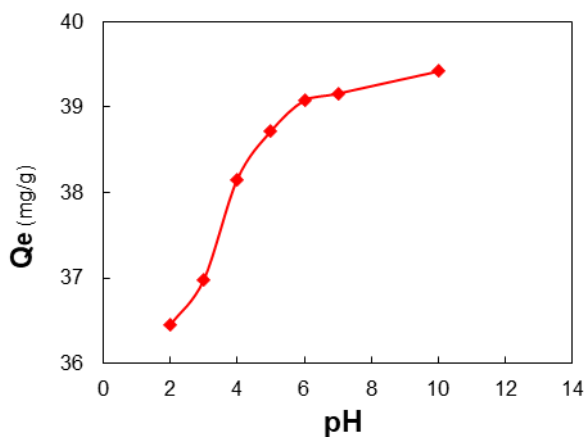


Fig. 13. Effect of acid function on RhB adsorption (t=120 min, V=10 mL, wt=0.05, C=200mg L⁻¹, T=25°C).

Table 2. The values of the thermodynamic functions of the RhB dye adsorption process on the surface of the adsorbent at 25°C.

| ΔH (kJ/mol) | ΔG (kJ/mol) | ΔS (kJ/K.mol) | Equilibrium Constant (K) |
|---------------------|---------------------|-----------------------|--------------------------|
| -24.188 | -6.544 | -60.217 | 5.872 |



which makes the surface contract, hindering the diffusion of dye molecules into the composite [77]. Additionally, repulsion between the -COOH, OH groups on the composite surface and the positive charge of the dye hinders the molecules' access to the surface, resulting in a decrease in the adsorption process[78].

CONCLUSION

Upon analyzing hydrogel nanocomposites, it was identified that the incorporation of MWCNTs-COOH enhanced the composite's porous structure, increasing adsorption capacity for RhB dye. The synthesized materials were analyzed using TEM, XRD, and TGA techniques. The FESEM results demonstrated increased surface smoothness due to dye molecule absorption. The TGA results showed the thermal stability of the hybrid materials was significantly improved compared to the CS-g-p(AA-co-DEAP) alone. XRD patterns confirmed a well-dispersed and uniform distribution of MWCNTs-COOH in the composite hydrogel matrix, confirming the capacity of nanostructures to accommodate structural deformations. Composite weight and MWCNTs-COOH concentration were investigated to identify optimal concentrations in the adsorption process. A Freundlich isotherm provided the best fit for the adsorption data, suggesting a multilayered, heterogeneous nature of the adsorbent surface. The effect of temperature on the adsorption process was noted, indicating an exothermic process, with a reduction in the degrees of freedom for adsorbed RhB dye molecules.

CONFLICT OF INTEREST

The authors declare that there is no conflict of interests regarding the publication of this manuscript.

REFERENCES

- Lellis B, Fávoro-Polonio CZ, Pamphile JA, Polonio JC. Effects of textile dyes on health and the environment and bioremediation potential of living organisms. *Biotechnology Research and Innovation*. 2019;3(2):275-290.
- Valian M, Salavati-Niasari M, Ganduh SH, Abdulsahib WK, Mahdi MA, Jasim LS. Sol-gel auto-combustion synthesis of a novel chitosan/Ho₂Ti₂O₇ nanocomposite and its characterization for photocatalytic degradation of organic pollutant in wastewater under visible illumination. *International Journal of Hydrogen Energy*. 2022;47(49):21146-21159.
- Dong S, Wang L, Lou W, Shi Y, Li L, Cao Z, et al. Synthesis of TiO₂/Bi-MOFs composites with excellent performance for enhanced visible-light driven photocatalytic activity to remove organic contaminants. *Journal of Dispersion Science and Technology*. 2022;44(11):2058-2069.
- Hiroki A, Taguchi M. Development of Environmentally Friendly Cellulose Derivative-Based Hydrogels for Contact Lenses Using a Radiation Crosslinking Technique. *Applied Sciences*. 2021;11(19):9168.
- Mahde BW, Sultan AM, Mahdi MA, Jasim LS. Kinetic Adsorption and Release Study of Sulfadiazine Hydrochloride Drug from Aqueous Solutions on GO/P(AA-AM-MCC) Composite. *INTERNATIONAL JOURNAL OF DRUG DELIVERY TECHNOLOGY*. 2022;12(04):1583-1589.
- Zhu L, Dong X-X, Gao C-B, Gai Z, He Y-X, Qian Z-J, et al. Development of a highly sensitive and selective electrochemical immunosensor for controlling of rhodamine B abuse in food samples. *Food Control*. 2022;133:108662.
- Mahmood Taher A, Ali Kadhim Kyhoiesh H, Shakir Waheeb A, Al-Adilee KJ, Jasim LS. Synthesis, characterization, biological activity, and modelling protein docking of divalent, trivalent, and tetravalent metal ion complexes of new azo ligand (N,N,O) derived from benzimidazole. *Results in Chemistry*. 2024;12:101911.
- Abdul-Rida NA, Talib KM. NEW CHALCONE DERIVATIVES AS ANTICANCER AND ANTIOXIDANT AGENTS: SYNTHESIS, MOLECULAR DOCKING STUDY AND BIOLOGICAL EVALUATION. *Chemical Problems*. 2024;22(2):177-186.
- Hamzah SK, Jabbar NK, Almzaiee AJ, Sabit RA. The Role Caspase-8 and DNA Methylation in patients with Ovarian Cancer: Relationship with Oxidative Stress and Inflammation. *Research Journal of Pharmacy and Technology*. 2021:2676-2680.
- da Cruz Severo E, Dotto GL, Martínez-de la Cruz A, Cuellar EL, Foletto EL. Enhanced photocatalytic activity of BiVO₄ powders synthesized in presence of EDTA for the decolorization of rhodamine B from aqueous solution. *Environmental Science and Pollution Research*. 2018;25(34):34123-34130.
- Mahdi MA, Oroumi G, Samimi F, Dawi EA, Abed MJ, Alzaidy AH, et al. Tailoring the innovative Lu₂CrMnO₆ double perovskite nanostructure as an efficient electrode materials for electrochemical hydrogen storage application. *Journal of Energy Storage*. 2024;88:111660.
- Sahib IJ, Aljeboree AM, Mahdi AB, Jasim LS, Alkaim AF. Highly efficient removal of toxic Pb(II) from aqueous solution by chitosan-g-p(AA-co-AAm) hydrogel: Kinetic, models. *AIP Conference Proceedings*: AIP Publishing; 2023. p. 040073.
- Synthesis, Characterization And Antibacterial Analysis Of Benzocaine Schiff Base Metal Complexes. *Nanotechnology Perceptions*. 2024;20(6).
- Khorasanizadeh MH, Hajizadeh-Oghaz M, Khoobi A, Ganduh SH, Mahdi MA, Abdulsahib WK, et al. Synthesis and characterization of HoVO₄/CuO nanocomposites for photodegradation of methyl violet. *International Journal of Hydrogen Energy*. 2022;47(46):20112-20128.
- Kang L-L, Zeng Y-N, Wang Y-T, Li J-G, Wang F-P, Wang Y-J, et al. Removal of pollutants from wastewater using coffee waste as adsorbent: A review. *Journal of Water Process Engineering*. 2022;49:103178.
- Sajeesh S, Sharma CP. Mucoadhesive hydrogel microparticles based on poly (methacrylic acid-vinyl pyrrolidone)-chitosan for oral drug delivery. *Drug Deliv*. 2010;18(4):227-235.
- Kianipour S, Razavi FS, Hajizadeh-Oghaz M, Abdulsahib WK, Mahdi MA, Jasim LS, et al. The synthesis of the P/N-type NdCoO₃/g-C₃N₄ nano-heterojunction as a high-performance photocatalyst for the enhanced photocatalytic degradation of pollutants under visible-light irradiation. *Arabian Journal of Chemistry*. 2022;15(6):103840.
- Rodriguez-Narvaez OM, Peralta-Hernandez JM, Goonetilleke

- A, Bandala ER. Treatment technologies for emerging contaminants in water: A review. *Chem Eng J.* 2017;323:361-380.
19. Hosseini M, Ghanbari M, Dawi EA, Mahdi MA, Ganduh SH, Jasim LS, et al. Investigations of nickel silicate for degradation of water-soluble organic pollutants. *International Journal of Hydrogen Energy.* 2024;61:307-315.
 20. Jamel HO, Jasim MH, Mahdi MA, Ganduh SH, Batool M, Jasim LS, et al. Adsorption of Rhodamine B dye from solution using 3-((1-(4-((1H-benzo[d]imidazol-2-yl)amino)phenyl)ethylidene)amino)phenol (BIAPEHB)/ P(AA-co-AM) composite. *Desalination and Water Treatment.* 2025;321:101019.
 21. Tan KB, Vakili M, Horri BA, Poh PE, Abdullah AZ, Salamatinia B. Adsorption of dyes by nanomaterials: Recent developments and adsorption mechanisms. *Sep Purif Technol.* 2015;150:229-242.
 22. Zhou Y, Zhang J, Wu D. Enhanced photocatalytic degradation of ciprofloxacin over Bi₂MoO₆/g-C₃N₄/BiFeO₃ heterojunction photocatalyst under visible light irradiation. *Mater Sci Semicond Process.* 2022;151:107011.
 23. Jasim LS, Aljeboree AM, Sahib IJ, Mahdi MA, Abdulrazzak FH, Alkaim AF. Effective adsorptive removal of riboflavin (RF) over activated carbon. *AIP Conference Proceedings: AIP Publishing;* 2022. p. 030030.
 24. Pereira AGB, Rodrigues FHA, Paulino AT, Martins AF, Fajardo AR. Recent advances on composite hydrogels designed for the remediation of dye-contaminated water and wastewater: A review. *Journal of Cleaner Production.* 2021;284:124703.
 25. Vunain E, Mishra AK, Mamba BB. Dendrimers, mesoporous silicas and chitosan-based nanosorbents for the removal of heavy-metal ions: A review. *Int J Biol Macromol.* 2016;86:570-586.
 26. Dubey R, Dutta D, Sarkar A, Chattopadhyay P. Functionalized carbon nanotubes: synthesis, properties and applications in water purification, drug delivery, and material and biomedical sciences. *Nanoscale advances.* 2021;3(20):5722-5744.
 27. Al-Masoudi NA, Kassim AG, Abdul-Reda NA. Synthesis of Potential Pyrimidine Derivatives via Suzuki Cross-Coupling Reaction as HIV and Kinesin Eg5 Inhibitors. *Nucleosides, Nucleotides and Nucleic Acids.* 2014;33(3):141-161.
 28. Nabeel AA-R, Adnan S, Jaber QAH. Development of Novel Imaging Fluorescent Agents Bearing Anti-Inflammatory Drugs: Synthesis, Structural Characterization and Evaluation of Biological Activity. *uss J Bioorg Chem.* 2020;46(4):620-626.
 29. Liu J, Liu G, Liu W. Preparation of water-soluble β -cyclodextrin/poly(acrylic acid)/graphene oxide nanocomposites as new adsorbents to remove cationic dyes from aqueous solutions. *Chem Eng J.* 2014;257:299-308.
 30. Ibrahim RK, Hayyan M, AlSaadi MA, Hayyan A, Ibrahim S. Environmental application of nanotechnology: air, soil, and water. *Environmental Science and Pollution Research.* 2016;23(14):13754-13788.
 31. Yu M, Gao M, Shen T, Zeng H. Single and simultaneous adsorption of rhodamine B and congo red from aqueous solution by organo-vermiculites. *J Mol Liq.* 2019;292:111408.
 32. Tang L, Cai Y, Yang G, Liu Y, Zeng G, Zhou Y, et al. Cobalt nanoparticles-embedded magnetic ordered mesoporous carbon for highly effective adsorption of rhodamine B. *Applied Surface Science.* 2014;314:746-753.
 33. Ding L, Zou B, Gao W, Liu Q, Wang Z, Guo Y, et al. Adsorption of Rhodamine-B from aqueous solution using treated rice husk-based activated carbon. *Colloids Surf Physicochem Eng Aspects.* 2014;446:1-7.
 34. Wanyonyi WC, Onyari JM, Shiundu PM. Adsorption of Congo Red Dye from Aqueous Solutions Using Roots of Eichhornia Crassipes: Kinetic and Equilibrium Studies. *Energy Procedia.* 2014;50:862-869.
 35. Samiei M, Abdolahinia ED, Fathi M, Barar J, Omid Y. Chitosan-based bioactive hydrogels for osteogenic differentiation of dental pulp stem cells. *J Drug Deliv Sci Technol.* 2022;73:103478.
 36. Li B, Xu X, Hu Z, Li Y, Zhou M, Liu J, et al. Rapid preparation of N-CNTs/P(AA-co-AM) composite hydrogel via frontal polymerization and its mechanical and conductive properties. *RSC advances.* 2022;12(30):19022-19028.
 37. Spectrophotometric Determination of Metoclopramide- HCl in the standard raw and it compared with pharmaceuticals. *Journal of Pharmaceutical Negative Results.* 2021;21(2).
 38. Atyaa AI, Radhy ND, Jasim LS. Synthesis and Characterization of Graphene Oxide/Hydrogel Composites and Their Applications to Adsorptive Removal Congo Red from Aqueous Solution. *Journal of Physics: Conference Series.* 2019;1234(1):012095.
 39. Amorim CR, Pavani TFA, Lopes AFS, Duque MD, Mengarda ACA, Silva MP, et al. Schiff bases of 4-Phenyl-2-Aminothiazoles as hits to new antischistosomal: Synthesis, in vitro, in vivo and in silico studies. *Eur J Pharm Sci.* 2020;150:105371.
 40. Synthesis and Characterization of Zinc(II), Cadmium(II) and Palladium(II) Complexes with the Thiophene-Derived Schiff Base Ligand. *American Chemical Society (ACS).*
 41. Jasim L, Radhy N, Jamel H. Synthesis and Characterization of Poly (Acryl Amide - Maleic Acid) Hydrogel: Adsorption Kinetics of a Malachite Green from Aqueous Solutions. *Eurasian Journal of Analytical Chemistry.* 2018;13(1b).
 42. Jasim LS, Abdulsahib WK, Ganduh SH, Radia ND. New Approach for Sulfadiazine Toxicity Management using Carboxymethyl Cellulose Grafted Acrylamide Hydrogel. *International Journal of Drug Delivery Technology.* 2020;10(02):259-264.
 43. Kareem Hamzah S. Study some biochemical parameters in pregnant women with hypertension. *Journal of Physics: Conference Series.* 2019;1234(1):012092.
 44. Lin Y, Hong Y, Song Q, Zhang Z, Gao J, Tao T. Highly efficient removal of copper ions from water using poly(acrylic acid)-grafted chitosan adsorbent. *Colloid Polym Sci.* 2017;295(4):627-635.
 45. Chatterjee S, Lee MW, Woo SH. Adsorption of congo red by chitosan hydrogel beads impregnated with carbon nanotubes. *Bioresour Technol.* 2010;101(6):1800-1806.
 46. Qi L, Xu H, Tang R, Liu L, Chen Y, Wen Q. Study on power generation and Congo red decolorization of 3D conductive PPy-CNT hydrogel in bioelectrochemical system. *International Journal of Hydrogen Energy.* 2022;47(37):16568-16579.
 47. Shah A, Arjunan A, Manning G, Batool M, Zakharova J, Hawkins AJ, et al. Sequential novel use of Moringa oleifera Lam., biochar, and sand to remove turbidity, E. coli, and heavy metals from drinking water. *Cleaner Water.* 2024;2:100050.
 48. Falsafi SR, Rostamabadi H, Assadpour E, Jafari SM. Morphology and microstructural analysis of bioactive-loaded micro/nanocarriers via microscopy techniques; CLSM/SEM/TEM/AFM. *Adv Colloid Interface Sci.* 2020;280:102166.
 49. Yu J, Lu Q, Zheng J, Li Y. Chitosan/attapulgite/poly(acrylic acid) hydrogel prepared by glow-discharge electrolysis plasma as a reusable adsorbent for selective removal of Pb²⁺ ions. *Iranian Polymer Journal.* 2019;28(10):881-893.
 50. Abou Taleb MF, Abou El Fadl FI, Albalwi H. Adsorption of toxic dye in wastewater onto magnetic NVP/CS nanocomposite hydrogels synthesized using gamma radiation. *Sep Purif Technol.* 2021;266:118551.
 51. Luo YL, Zhang CH, Chen YS, Yang W. Preparation and

- characterisation of polyacrylamide/MWCNTs nanohybrid hydrogels with microporous structures. *Mater Res Innovations*. 2009;13(1):18-27.
52. Ali HE, Nasef SM, Gad YH. Remediation of Astrazon blue and Lerui acid brilliant blue dyes from waste solutions using amphoteric superparamagnetic nanocomposite hydrogels based on chitosan prepared by gamma rays. *Carbohydr Polym*. 2022;283:119149.
 53. Xu P, Zheng M, Chen N, Wu Z, Xu N, Tang J, et al. Uniform magnetic chitosan microspheres with radially oriented channels by electrostatic droplets method for efficient removal of Acid Blue. *Journal of the Taiwan Institute of Chemical Engineers*. 2019;104:210-218.
 54. Jamali M, Akbari A. Facile fabrication of magnetic chitosan hydrogel beads and modified by interfacial polymerization method and study of adsorption of cationic/anionic dyes from aqueous solution. *Journal of Environmental Chemical Engineering*. 2021;9(3):105175.
 55. Dawar N, Devi J, Kumar B, Dubey A. Synthesis, Characterization, Pharmacological Screening, Molecular Docking, DFT, MESP, ADMET Studies of Transition Metal(II) Chelates of Bidentate Schiff Base Ligand. *Inorg Chem Commun*. 2023;151:110567.
 56. Alwan Altaa SH, Habeeb Alshamsi HA, Jasim Al-Hayder LS. Synthesis and characterization of rGO/Co₃O₄ composite as nano-adsorbent for Rhodamine 6G dye removal. *Desalination and Water Treatment*. 2018;114:320-331.
 57. Zeng T, Hu X-q, Wu H, Yang J-w, Zhang H-b. Microwave assisted synthesis and characterization of a novel bio-based flocculant from dextran and chitosan. *Int J Biol Macromol*. 2019;131:760-768.
 58. Varshney A, Mishra AP. Synthesis, spectral characterization, computational studies, antifungal, DNA interaction, antioxidant and fluorescence property of novel Schiff base ligand and its metal chelates. *Spectrochimica Acta Part A: Molecular and Biomolecular Spectroscopy*. 2023;297:122765.
 59. Sethy TR, Pradhan AK, Sahoo PK. Simultaneous studies on kinetics, bio-adsorption behaviour of chitosan grafted thin film nanohydrogel for removal of hazardous metal ion from water. *Environmental Nanotechnology, Monitoring & Management*. 2019;12:100262.
 60. Abbas SS, Jasim LS. Removal of rhodamine B from aqueous solution by montmorillonite/poly (malic acid-co-acrylic acid): Thermodynamic study. *AIP Conference Proceedings: AIP Publishing*; 2023. p. 020013.
 61. Tian J, Fan R, Zhang Z, Li Y, Wu H, Yang P, et al. Flexible and biocompatible poly (vinyl alcohol)/multi-walled carbon nanotubes hydrogels with epsilon-near-zero properties. *Journal of Materials Science & Technology*. 2022;131:91-99.
 62. Batool M, Haider MN, Javed T. Applications of Spectroscopic Techniques for Characterization of Polymer Nanocomposite: A Review. *Journal of Inorganic and Organometallic Polymers and Materials*. 2022;32(12):4478-4503.
 63. Majeed HJ, Idrees TJ, Mahdi MA, Abed MJ, Batool M, Yousefi SR, et al. Synthesis and application of novel sodium carboxy methyl cellulose-g-poly acrylic acid carbon dots hydrogel nanocomposite (NaCMC-g-PAAc/ CDs) for adsorptive removal of malachite green dye. *Desalination and Water Treatment*. 2024;320:100822.
 64. Khalil H, Wadi VS, Hegab HM, Nassar L, Naddeo V, Yousef AF, et al. High-performance f-GO/MWCNTs-COOH nanohybrid-based polylactic acid mixed matrix membrane for wastewater treatment. *Journal of Water Process Engineering*. 2023;53:103784.
 65. Wu L, Li L, Fan M, Tang P, Yang S, Pan L, et al. Strong and tough PVA/PAA hydrogel fiber with highly strain sensitivity enabled by coating MWCNTs. *Composites Part A: Applied Science and Manufacturing*. 2020;138:106050.
 66. Mallakpour S, Rashidimoghadam S. Preparation, characterization, and in vitro bioactivity study of glutaraldehyde crosslinked chitosan/poly(vinyl alcohol)/ascorbic acid-MWCNTs bionanocomposites. *Int J Biol Macromol*. 2020;144:389-402.
 67. Foroutan R, Peighambaroust SJ, Esvandi Z, Khatooni H, Ramavandi B. Evaluation of two cationic dyes removal from aqueous environments using CNT/MgO/CuFe₂O₄ magnetic composite powder: A comparative study. *Journal of Environmental Chemical Engineering*. 2021;9(2):104752.
 68. Maneerung T, Liew J, Dai Y, Kawi S, Chong C, Wang C-H. Activated carbon derived from carbon residue from biomass gasification and its application for dye adsorption: Kinetics, isotherms and thermodynamic studies. *Bioresour Technol*. 2016;200:350-359.
 69. Inyinbor AA, Adekola FA, Olatunji GA. Kinetics, isotherms and thermodynamic modeling of liquid phase adsorption of Rhodamine B dye onto Raphia hookerie fruit epicarp. *Water Resources and Industry*. 2016;15:14-27.
 70. Aljeboree AM, Noor Alshirifi A. Oxidative coupling of Amoxicillin using 4-Aminoantipyrine: Stability and higher sensitivity. *Journal of Physics: Conference Series*. 2019;1294(5):052001.
 71. Lamrani O, Tanji K, Redouane H, Fahoul Y, Belkasmı M, Boushaba A. Efficient adsorption of RhB using Moroccan natural clay: equilibrium, kinetic, thermodynamic, and theoretical study. *Euro-Mediterranean Journal for Environmental Integration*. 2023;8(2):303-318.
 72. Ali F, Ali N, Bibi I, Said A, Nawaz S, Ali Z, et al. Adsorption isotherm, kinetics and thermodynamic of acid blue and basic blue dyes onto activated charcoal. *Case Studies in Chemical and Environmental Engineering*. 2020;2:100040.
 73. Gharbani P, Mehrizad A. Preparation and characterization of graphitic carbon nitrides/polyvinylidene fluoride adsorptive membrane modified with chitosan for Rhodamine B dye removal from water: Adsorption isotherms, kinetics and thermodynamics. *Carbohydr Polym*. 2022;277:118860.
 74. Liu Y, Zheng Y, Wang A. Enhanced adsorption of Methylene Blue from aqueous solution by chitosan-g-poly (acrylic acid)/vermiculite hydrogel composites. *Journal of Environmental Sciences*. 2010;22(4):486-493.
 75. Vigneshwaran S, Sirajudheen P, Karthikeyan P, Meenakshi S. Fabrication of sulfur-doped biochar derived from tapioca peel waste with superior adsorption performance for the removal of Malachite green and Rhodamine B dyes. *Surfaces and Interfaces*. 2021;23:100920.
 76. Bhattacharyya A, Banerjee B, Ghorai S, Rana D, Roy I, Sarkar G, et al. Development of an auto-phase separable and reusable graphene oxide-potato starch based cross-linked bio-composite adsorbent for removal of methylene blue dye. *Int J Biol Macromol*. 2018;116:1037-1048.
 77. Shaikh WA, Islam RU, Chakraborty S. Stable silver nanoparticle doped mesoporous biochar-based nanocomposite for efficient removal of toxic dyes. *Journal of Environmental Chemical Engineering*. 2021;9(1):104982.
 78. Nakhjiri MT, Bagheri Marandi G, Kurdtabar M. Adsorption of Methylene Blue, Brilliant Green and Rhodamine B from Aqueous Solution Using Collagen-g-p(AA-co-NVP)/Fe₃O₄@SiO₂ Nanocomposite Hydrogel. *J Polym Environ*. 2019;27(3):581-599.